Combination of interfacial reduction of hexavalent chromium and trivalent chromium immobilization on tin-functionalized hydroxyapatite materials

Sebastiano Campisi, Claudio Evangelisti, Georgeta Postole, Antonella Gervasini

Combination of interfacial reduction of hexavalent chromium and trivalent chromium immobilization on tin-functionalized hydroxyapatite materials

Sebastiano Campisi [a], Claudio Evangelisti [b], Georgeta Postole [c], Antonella Gervasini [a,*]

[a] *Dipartimento di Chimica, Università degli Studi di Milano, via Camillo Golgi 19, I-20133 Milano, Italy*
[b] *CNR - ICCOM - Istituto di Chimica dei Composti OrganoMetallici, Via G. Moruzzi 1, I-56124 Pisa, Italy*
[c] *Univ Lyon, Université Claude Bernard Lyon 1, CNRS, IRCELYON, F-69626 Villeurbanne, France*

We present an ecofriendly hydroxyapatite (HAP) material functionalized with tin (Sn/HAP) for an efficient interfacial reduction of Cr(VI) to Cr(III).

Tin was deposited on HAP at different concentrations (from 0.2 to 1.2 mmol/g) using colloidal or clear acid solutions of $SnCl_2$. The morphological and structural properties of fresh and used Sn/HAP samples were determined (N_2 adsorption-desorption, transmission electron microscopy techniques, XRPD, XPS). Tests were performed under various conditions: at different pH 3–7, inert or oxidant atmosphere, sample aging (up to 15 days).

Sn/HAP samples prepared using colloidal acid solutions revealed the best performances in the reduction of Cr (VI) to Cr(III), carried out under mild conditions (40 °C in acidified solution) with initial concentration of Cr(VI) in the range from 25 to 50 ppm. Best removal of Cr(VI) (10 mg/g) was obtained by using a Sn-concentration of 0.65 mmol/g with complete adsorption of the formed Cr(III) at HAP surface. This finding was associated with higher Sn-dispersion (surface Sn, 9.4 at.%) compared to samples prepared from clear solutions (surface, Sn 7.7 at. %), as evidenced by HAADF-STEM/EDX and XPS analyses. Remarkably, tin was tightly retained on the HAP surface under reaction conditions (0.7% leaching), confirming the occurrence of Cr(VI) reduction at solid-liquid interphase.

1. Introduction

In the environment matrices chromium typically occurs in two oxidation states: Cr(III) and Cr(VI), which differ in several chemical and physical properties. Cr(III) is a micronutrient, characterized by a low mobility and limited biological uptake, thereby it is considered non-toxic at low concentration. In addition, it can be readily removed from solutions by precipitation as solid (oxy)-hydroxide phase over the pH range of most natural resources. On the contrary, hexavalent chromium, Cr(VI), can form different species in aqueous solutions such as hydrogen chromate ($HCrO_4^-$), chromate (CrO_4^{2-}), and dichromate ($Cr_2O_7^{2-}$), whose relative distribution is a function of pH, redox potential and Cr(VI) concentration. All these species have high solubility in water (also in alkaline conditions) and high mobility. Due to these properties, remarkable diffusivity of Cr(VI) through soil and aquatic environments as well as capability to cross biological membranes can occur. The latter factor is probably the basis of the well-documented adverse human health effects both at short-term and long-term exposures [1].

Besides biogenic contamination related to naturally occurring Cr(VI) in minerals and sediments, Cr(VI) in the environment originates in large part from anthropogenic activities, because of its wide range of industrial applications, including catalysis, metal plating, tanning, wood treatment, paint production, corrosion inhibition, industrial water cooling, paper pulp production, and petroleum refining. Depending on the specific source, the concentration of Cr(VI) in industrial wastewaters (in the absence of any pre-treatment) can be between 10 and 4000 $mg{\cdot}L^{-1}$ ($1\ mg{\cdot}L^{-1} = 1$ ppm) [2].

Considering the high toxicity of Cr(VI), the maximum allowable limit for total chromium is strictly regulated by governments and regulatory agencies. The legal discharge limits for total Cr vary in different countries and depending on some operative conditions (e.g. water mass flow); limit values between 0.005 and 2 $mg{\cdot}L^{-1}$ are generally found for industrial wastewaters [3].

Unfortunately, a direct precipitation method cannot be applied for removal of Cr(VI) from water, since all Cr(VI) species do not form insoluble precipitates. Therefore, in order to meet the increasingly

* Corresponding author.
E-mail address: antonella.gervasini@unimi.it (A. Gervasini).

stringent emission standard, alternative Cr(VI) remediation technologies [2,4,5] have been proposed based on chemical transformations (chemical or photochemical reduction, ion exchange, adsorption), biological transformations (phytoremediation, microbial reduction) or physical processes (membrane filtration, *in situ* electro-kinetics).

Among these conventional technologies the most practical solution is based on adsorption, which offers significant advantages like low energy consumption, easiness of operation and cost-effectiveness [5]. However, most effective adsorbents (e.g. activated carbons, zeolites, polymeric resins) often suffer from high production costs and/or difficult regeneration. Furthermore, both natural and synthetic conventional adsorbents are not completely effective in the removal of Cr(VI) and further modification of these materials is necessary to boost the adsorption capacities. From this point of view, a successful Cr removal strategy, based on the synergistic combination of reduction and adsorption processes, has been proposed in the literature in the last decade [5]. This approach originated from the evidence that iron-containing minerals, such as magnetite [6], Fe(II)-rich goethite [7] and Fe(II)-rich biotite [8], could act as solid-phase reductants able to promote, by electron transfer, the heterogeneous reduction of Cr(VI) to strongly-adsorbing Cr(III) at the interphase [6].

Based on these results several iron-containing solid materials have been successfully employed in simultaneous reductive and sorptive removal of Cr(VI) [9–13]. Usually, the iron phase was immobilised onto a support, as in the case of Fe(0) nanoparticles (NPs) supported on reduced graphene oxide-alginate beads [10], layered double hydroxide (LDH) decorated reduced graphene oxide [14], polyvinylalcohol-alginate beads [15] or β-FeOOH precipitated on a soybean meal-derived activated carbon [12]. More sophisticated systems have been also designed, such as carbon/ferrous sulfide/iron (C/FeS/Fe) composites or sandwich-like nanostructures consisting of two pieces of waste cotton fabrics (CFs) supporting ferrous sulfide (FeS) and carboxyl-functionalized ferroferric oxide (CFFM) respectively [13]. In addition, another class of iron-based materials has attracted a great interest, namely functionalized Fe_3O_4 NPs. This class of organic-inorganic materials combines the reduction and adsorption properties of an organic ligand (e.g. polypyrrole [16], poly(m-phenylenediamine) [17], gallic acid [18], humic acid [19]) and the advantages of easy separation imparted by the magnetic properties of Fe_3O_4 NPs. Besides iron-containing materials, the coupled reduction-adsorption process has been demonstrated to occur over several polymeric matrices (e.g. ethyl cellulose-polyethylenimine composites [20]), inorganic materials (e.g. mesoporous silicas [21], titanium carbides [22], noble metal NPs [23]), biomaterials [24–26] and biocomposites (e.g. triazine assisted microporous covalent organic polymer enfolded alginate biocomposite beads) [27]. Furthermore, the combination of adsorption with photocatalytic [28–33] or electrochemical [4,34–36] reduction has been also explored. Despite the unique performances in Cr(VI) removal by these materials, extensive efforts are also required to develop eco-friendly, effective and reusable materials.

Calcium hydroxyapatite (HAP) is an interesting solid belonging to hydroxyapatite family with formula $Ca_{10-x}(PO_4)_{6-x}(HPO_4)_x(OH)_{2-x}$ (with $0 < x < 1$). Because of the unique properties of bioavailability, biocompatibility, low cost, thermal stability, and water insolubility ($K_{ps} \approx 10^{-59}$ at room temperature), HAP represents a cheap and eco-friendly material which can found multiple applications in the field of environmental protection [37]. In particular, thanks to its functionalized surface (phosphate and hydroxyl groups, in particular) and the ion exchange-properties, HAP can act as sorbent towards several heavy metal ions [38–40].

Although few studies [41–43] reported the uptake of Cr(VI) on HAP, our preliminary capture tests demonstrated that Cr(VI) removal cannot be carried out by a simple contact of water containing chromate/bichromate species with HAP surface. On the other hand, we proved that hydroxyapatite is able to retain up to 99% of the Cr(III) present in the solution in a large range of pH (4–9) and concentration (15–300 ppm) [39].

This remarkable affinity of HAP towards Cr(III) encouraged us to design a novel material encompassing the sorbent feature of HAP in combination with the reducing power of a metal species in order to accomplish the reduction/adsorption process.

Besides ferrous salts, stannous salts (in powder or liquid form) have been extensively employed for the chemical reduction of Cr(VI) to Cr (III) [44], which proceeds according to Eq. (1):

$$3Sn^{2+} + Cr_2O_7^{2-} + 14H^+ \rightarrow 3Sn^{4+} + 2Cr^{3+} + 7H_2O \qquad E^\circ = 1.18V(25\ ^\circ C) \tag{1}$$

Nevertheless, unlike the iron, only few studies focused on the application of Sn-based materials in the reduction/adsorption of Cr(VI) [45–48].

In this work, the chemical reduction described by Eq. (1) has been heterogenized and coupled with an adsorption of the formed Cr^{3+} species, by using a novel material consisting of hydroxyapatite (HAP) functionalized with Sn(II). Sn-functionalized HAP samples (Sn/HAP) with different Sn concentration (2.5 wt.% < [Sn] < 10 wt.%) were prepared using different Sn-solutions and surface properties of synthesized materials have been determined before and after use. Numerous tests of Cr(VI) removal were performed varying operating conditions: pH values, initial Cr(VI) concentration, as well as atmosphere to probe the reductive and adsorptive capacity of the samples and to study the influence of Sn loading and its surface concentration on activity. Targeted tests of Sn-leaching from Sn/HAP and characterization analyses by transmission electron microscopy (TEM), high angular annular dark field scanning transmission electron microscopy (HAADF-STEM) along with energy-dispersive X-ray (EDX) analysis, and X-ray photoelectron spectroscopy (XPS) provided evidences for the occurrence of the heterogeneous redox *plus* adsorption phenomena at the chromium-Sn/HAP aqueous interphase.

2. Materials and methods

2.1. Materials

Hydroxyapatite (calcium phosphate tribasic) powder was provided by Alfa Aesar. Tin chloride dihydrate ($SnCl_2{\cdot}2H_2O$, ≥98.0% oxidimetric assay), chromium chloride hexahydrate ($CrCl_3{\cdot}6H_2O$, ≥98.0% oxidimetric assay) and potassium bichromate ($K_2Cr_2O_7$, ≥99.0% oxidimetric assay) salts of analytical grade were purchased from Carlo Erba (RPE purity). Hydrochloric acid (37 wt.% and 0.5 $mol{\cdot}L^{-1}$ < 1 ppm of heavy metal content), 2-propanol (purity greater than 99.5%), acetone (purity GC, ≥99.8%) and 1,5-diphenylcarbazide (DPC, purity DSC ≥ 98.0%) were from Merck. MilliQ water previously de-aerated was used in all the experiments, while HPLC-grade Water from Merck was used for all the analyses. Nitrogen, 99.9995% purity from SAPIO was used as inert gas.

2.2. Preparation of Sn-functionalized hydroxyapatite

Sn with nominal concentration from 2.5 to 10 wt.% (0.2–1.2 $mmol_{Sn}{\cdot}g^{-1}$) was deposited on HAP from *i)* colloidal Sn-solution (pH = 2) and *ii)* clear Sn-solution (pH = 1) using a technique already validated for deposition of Cu(II) and Fe(III) species on HAP [49,50]. Aqueous solutions of $SnCl_2{\cdot}2H_2O$ having proper Sn-concentration were put in a 250 mL *3-neck* flask, immersed in a water bath thermostated at 40 °C under nitrogen flow. To prepare the first series of samples (Sn/HAP_{coll}), HCl (37 wt.%) was added to $SnCl_2{\cdot}2H_2O$ solutions to obtain the pH value of 2; in this case, the observed solutions were slightly opaque. A second series of samples (Sn/HAP_{sol}) was prepared at pH = 1; in this case the solutions were clear. Then, a proper amount of dried and weighted HAP powder was put into the acidic solutions. The suspensions were kept under stirring at 40 °C for 15 min. The final pH of the solutions was always about 6–7. Then, the solids were recovered by filtration and

dried at 120 °C in a static vacuum oven overnight. All the samples have been maintained in capped test tubes under nitrogen atmosphere. Sn loading was verified through ICP-OES analysis on digested solid and in general, the actual Sn-loading values were affected by ±6.5% *bias*.

Sn-leaching tests at different pH values were performed by dispersing 0.1 g of sample in 10 mL of MilliQ water. The pH was adjusted using hydrochloric acid (pH = 3, pH = 5) or sodium hydroxide solution (pH = 7, pH = 9). After a given contact time (1 h, 2 h, 4 h), the solid was separated by centrifugation and the solution was analysed by inductively coupled plasma optical emission spectroscopy (ICP-OES) to quantify the leached Sn from Sn/HAP.

2.3. Physico-chemical characterization

Sn loading was determined by inductively coupled plasma optical emission spectroscopy (ICP-OES) with an ACTIVA spectrometer from Horiba JOBIN YVON.

ZEISS LIBRA 200FE microscope with a 200 kV FEG source, in column second-generation omega filter was used for transmission electron microscopy (TEM). Chemical analysis was performed using HAADF-STEM (high angular annular dark field scanning transmission electron microscopy) facility and Energy-dispersive X-ray (EDX) probe (Oxford INCA Energy TEM 200). EDX spectra and element maps were collected along with HAADF-STEM micrographs.

N_2-adsorption-desorption isotherms were collected at the liquid nitrogen temperature on a Sorptomatic 1990 (by Thermo Scientific). The analysis was managed by MILES-200 program and the MILEADP software was used for the elaboration.

X-Ray powder diffraction (XRPD) patterns have been collected using a PANalytical XPert PRO powder diffractometer operating with an X-ray source at 40 kV and 25 mA in the range between 5°- 65°(2θ), step of 0.033° 2θ and collection time of 50 s.

Fourier Transform Infrared spectra (FT-IR) were collected in the wavenumber interval between 400 cm^{-1} and 4000 cm^{-1} at room temperature in a Perkin-Elmer Spectrum Two FT-IR spectrometer. Before the analysis, the samples were dried at 120 °C overnight and then pelletized with dried KBr (sample to KBr weight ratio ca. 1:30).

XPS spectra were acquired by a KRATOS AXIS ULTRA DLD spectrometer (Kratos Analytical) equipped with a magnetic immersion lens, a hemispherical analyzer and a delay line detector.

2.4. Chromium reduction-immobilization tests

Stock solutions of Cr(VI) with concentration in the range 20–50 ppm were prepared by dissolving weighed amount of $K_2Cr_2O_7$ in MilliQ water. Then 20 mL of stock Cr(VI) solution were transferred in a 50 mL three-necks round flask and thermostatted at 40 °C. Approximately 0.1 g of weighed dried Sn/HAP powder was added (dosage 4 $g{\cdot}L^{-1}$) to the three-necks round flask and the stirred suspension was maintained under inert (N_2) or oxidative (air) fluxing. Finally, the pH = 3 was achieved by dropping 2 mL of 0.1 M hydrochloric acid, except for the tests at natural pH (pH *ca.* 7), where 2 mL of MilliQ water were added to maintain unaltered the Sn/HAP dosage. After 4 h of reaction, the mixture was then filtered under vacuum. The solution was stored and diluted for analysis while the solid was recovered and dried under vacuum at 120 °C overnight.

Similar procedure was followed for the tests with variable experimental conditions, performed in a home-made parallel tube reaction station (7 positions, 50 mL volume tubes). In this case, at the end of reaction, the solid was separated from the solution by centrifugation at 3500 rpm (15 min).

On a selected sample (Sn/HAP_{coll} with Sn at 7.5 wt.%), tests of reaction rate have been carried out at different temperatures. For the test, the following conditions were used: initial Cr(VI) concentration of 100 ppm, 4 g L^{-1} dosage, pH = 3, for 2 h under stirring in air atmosphere, at temperature interval from 5 °C to 40 °C by using a thermocriostat (Lauda Model K2R).

In some cases, the recovered and dried solid was re-used in successive runs under the same experimental conditions of the first one ([Cr (VI)]° = 50 ppm, pH = 3, 40 °C, in nitrogen fluxing), to assess the reusability of Sn/HAP materials.

The residual concentration of Cr(VI) in the solution was determined by UV−vis spectrophotometric analysis working at 540 nm by using 5-diphenyl carbazide (DPC) method [51] (see paragraph S.1 of S.I. for details).

The total concentration of Cr was measured by ICP-OES. In addition, the total amount of Cr immobilized on the Sn/HAP samples was also determined by ICP-OES after solid digestion in HCl 37 wt.%. To determine the performance of the Sn/HAP samples in the process, double check analyzes were performed, as follows: Cr (VI) removed from the solution was quantified by measuring i) the initial and residual concentrations of Cr(VI) in the solutions and ii) the amount of Cr(III) immobilized on the recovered sample from activity tests, after acid digestion. In any case, the two approaches were in excellent agreement and the material balance for chromium was very satisfactory.

The performances have been evaluated in terms of percent efficiency (%) or removal capacity ($mg_{Cr}{\cdot}g^{-1}$) from the residual Cr(VI) concentration in solution and from Cr(III) concentration immobilized at hydroxyapatite surface, respectively (equations are reported in paragraph S.1 of S.I.)

All the tests were repeated three times to assess reproducibility. In most cases, percent errors were smaller than 5%.

3. Results and discussion

3.1. Preparation and properties of Sn-HAP samples

Commercial stoichiometric hydroxyapatite (Ca/P ratio = 1.69, as determined by ICP-OES analysis) with needle-shaped nanocrystals and mesoporous structure (Fig. S-1) has been functionalized by deposition of dispersed tin phase. Aqueous acid solutions of $SnCl_2$ dihydrate in concentration range between 2 and 10 mM were prepared to obtain samples with a final Sn loading between 2.5 and 10 wt.%.

According to Sn speciation curve [52,53], the pH of Sn-containing solution should preferably be less than 3 to prevent the rapid nucleation and growth of insoluble $Sn(OH)_2$ in solution. In this study, the results obtained for Sn-solutions at pH = 1 and pH = 2 are presented. A different Sn speciation could be assumed in the resulting solutions: the dissolution of tin chloride at pH = 1 produced clear and colorless solutions, whereas solutions at pH = 2 appeared as milky white colloidal solutions (Fig. 1A).

High-resolution TEM analysis of Sn-colloidal solution showed the presence of nanocrystalline particles with particle sizes ranging between 2 and 3 nm (see Fig. 1B and Fig. S-2). Lattice planes extended to the whole particle, indicating their single crystalline nature. Electron diffraction analysis revealed rings in the FT pattern at 3.5, 2.6 and 1.8 Å (Fig. 1C). The observed signals can be tentatively ascribed to the spacing of (1 1 2), (3 1 0) and (5 1 0) planes, respectively, of monoclinic $SnCl_2$ [54], obtained by dehydration, under the analysis conditions, of the starting $SnCl_2(OH_2)$ [55].

By contacting HAP powder alternatively with colloidal or clear Sn-solutions, two series of samples have been obtained, named SnX/HAP_{coll} and SnX/HAP_{sol}, respectively (where X symbolizes the nominal Sn loading in wt.%). The tin-loading determined by ICP-OES, was in agreement with nominal values with an average discrepancy of 6.5%.

The morphological investigation revealed that in both cases the deposition of Sn caused a decrease of surface area (ca. 40%) in comparison with pristine HAP (76 $m^2{\cdot}g^{-1}$) (Fig. 1D and Fig. S-1). The Sn/HAP samples maintained mesoporosity with a slight pore volume increase (from 0.22 for bare HAP to 0.25 and 0.26 $cm^3{\cdot}g^{-1}$ for $Sn7.5/HAP_{coll}$ and $Sn7.5/HAP_{sol}$, respectively, Table S1). The decrease in surface area could be ascribed to a partial aggregation of hydroxyapatite

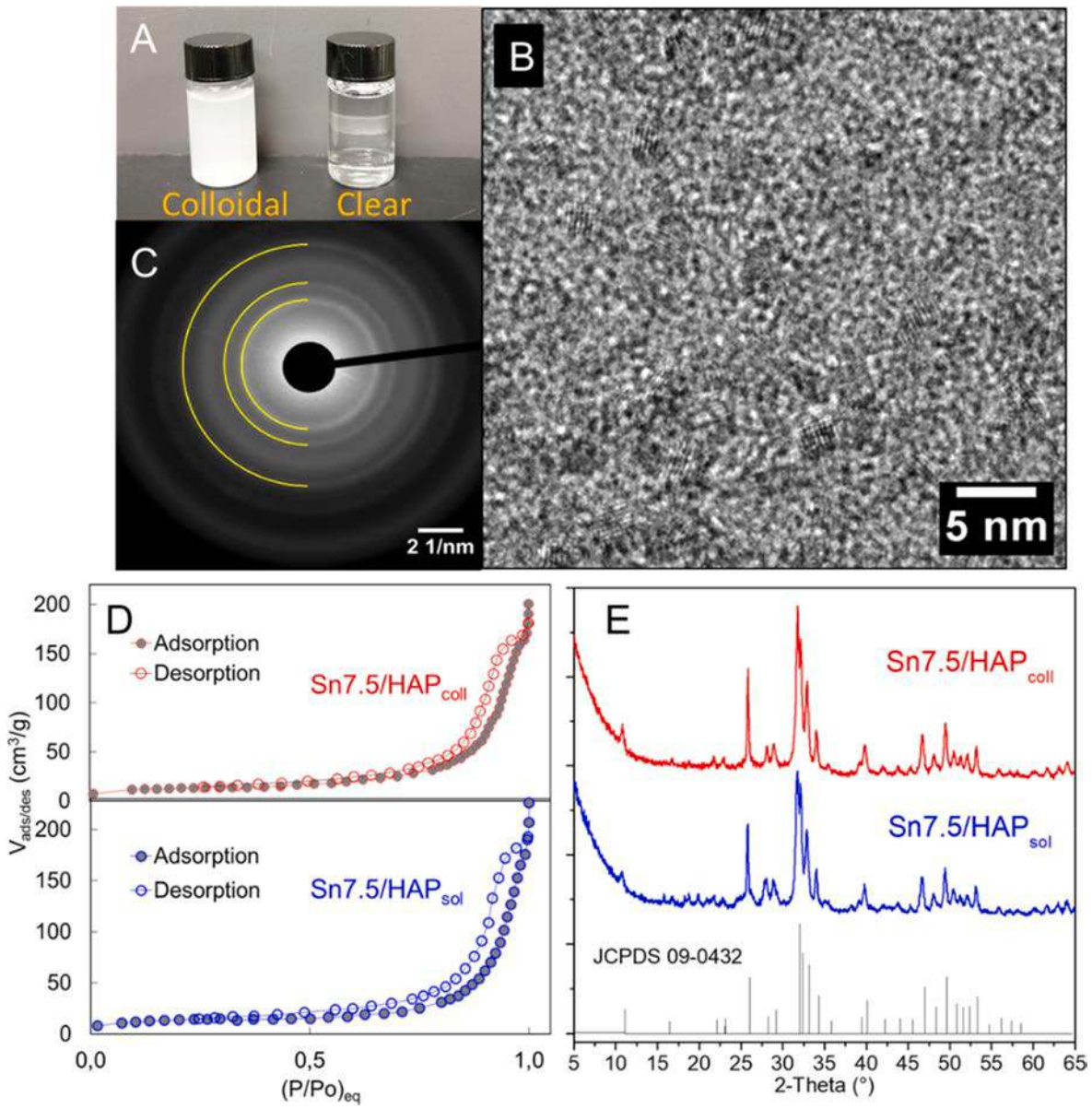

Fig. 1. Pictures of colloidal and clear acid solutions of $SnCl_2{\cdot}2H_2O$ used for the HAP functionalization (A); high resolution TEM micrograph (B) and electron diffraction pattern of Sn-colloidal (C); N_2 adsorption/desorption isotherms on Sn7.5/HAP_{coll} and Sn7.5/HAP_{sol} (D); XRPD of selected Sn-samples: Sn7.5/HAP_{coll} and Sn7.5/HAP_{sol} (E).

nanocrystals to form secondary agglomerate under the harsh conditions underwent during the preparation of Sn/HAP samples. Although highly acidic environment might also cause partial dissolution or structural changes of HAP, in our case the short contact time allowed to preserve the crystalline structure of HAP even after Sn deposition, as demonstrated by the X-ray powder diffractograms (Fig. 1E) and FT-IR spectra (Fig. S-3). Actually only one crystal phase (indexed as hexagonal hydroxyapatite according to the JCPDS 09-0432) was identified in collected XRPD patterns and no other calcium phosphate phases were present. Infrared spectroscopic analysis of HAP before and after Sn-functionalization (Fig. S-3) showed the fundamental vibrational modes of the hydroxyapatite phase. In particular, three main spectral contributions can be identified: i) vibrational modes of phosphate species (565 cm^{-1}, 605 cm^{-1}, 963 cm^{-1} and 1030–1100 cm^{-1}); ii) carbonate bands (1300–1600 cm^{-1}) ascribable to partial substitution of apatite anionic groups (PO_4^{3-} and OH^-) with carbonate anions; iii) high-energy region bands associated with adsorbed/constitutive water molecules and hydroxyl groups (3300–3700 cm^{-1}). The absence of any significant perturbation of the IR bands of HAP after functionalization with tin phase provided further evidence that any compositional or structural HAP modifications did not occur.

The Sn/HAP samples were investigated by HAADF-STEM microscopy. The Sn7.5/HAP_{coll} sample showed prismatic HAP structures homogeneously decorated by nanoparticles onto their surface (Fig. 2A). The particles sizes were comparable to those observed in the starting colloidal solution (d = 2–3 nm). EDX analysis indicated that these structures included Sn without any chloride species. This unexpected result can be justified considering the occurrence of an anion-exchange process between chloride and phosphate anions. It is well known that HAP is vulnerable in acidic solutions and tends to release phosphate at the interface where the anion exchange can occur without any modification of Sn-morphology. Furthermore, from the HAADF-STEM /EDX map in Fig. 2B (and in more complete feature in Fig. S-4) it is observed that these Sn-containing particles are homogeneously dispersed in the investigated area.

On the other hand, in the Sn7.5/HAP_{sol} sample HAADF-STEM

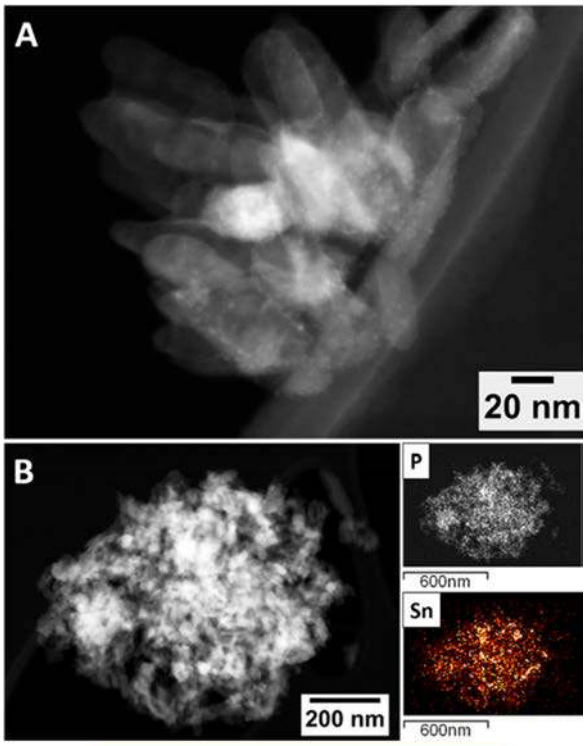

EDX Composition mol. (%)			
Ca	Sn	P	O
17.6	1.9	15.1	65.4

Fig. 2. HAADF-STEM micrograph at high magnification (A) and HAADF-STEM/EDX mapping of P and Sn (B) of the Sn7.5/HAP_{coll} sample.

micrographs (Fig. 3 and Fig. S-5) revealed the presence of hydroxyapatite crystals decorated with a minor fraction of Sn-based NPs (area 1, Fig. 3), similar to those observed in the sample prepared from colloidal solution, together with a major amount of a segregated crystalline phase containing a high fraction of Sn (area 2, Fig. 3 and Fig. 4 and Fig. S-6).

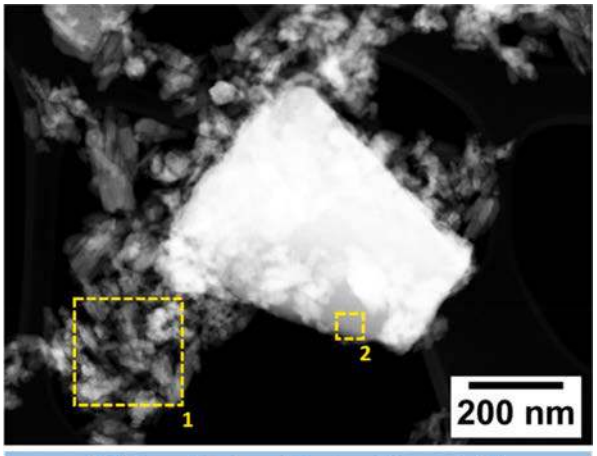

EDX Sampling Area / Composition mol. (%)							
1				2			
Ca	Sn	P	O	Ca	Sn	P	O
18.8	1.2	15.9	64.1	3.1	6.9	21.7	69.3

Fig. 3. HAADF-STEM micrograph of Sn7.5/HAP_{sol} sample and EDX semi-quantitative analysis of the areas selected on the image.

Based on the diffraction pattern (Fig. S-7), this phase might be ascribed to the growth of $SnHPO_4$. The formation of $SnHPO_4$ from the interaction of tin halide and hydroxyapatite at a low pH value is reported in the literature as a consequence of a partial dissolution of HAP in acidic media with release of phosphate ions at the interphase [56]. The calculated interplanar distances of the detected phase compared well with those of $SnHPO_4$ even if a clear assignation is not possible. However, this observation indicated that the contact between the acid solution and HAP surface can lead to its dissolution at some extent and to the formation of surface layers of new phases based on tin phosphates.

Ultimately, depending on the initial pH values of the $SnCl_2$ solution (pH = 1 or pH = 2), different Sn/HAP materials with different structure and aggregation state of the Sn phase have been obtained (Scheme 1).

It is noteworthy, as observed from Sn leaching tests in aqueous solution at different pH values, that for both the Sn/HAP_{sol} series of samples and the Sn/HAP_{coll} series, the Sn phase, once immobilized, remained strongly held on the HAP surface. Sn-leaching from Sn/HAP samples in aqueous solutions was negligible (<3%) in a wide range of pH values (Fig. S-8).

3.2. Chromium reduction-immobilization results

3.2.1. Effect of Sn loading and preparation method

The performances of the samples of the Sn/HAP_{coll} and Sn/HAP_{sol} series were studied in batch tests, operating under typical conditions: $[Cr(VI)]^{\circ}$=50 $mg{\cdot}L^{-1}$, pH = 3, Sn/HAP dosage = 4 $g{\cdot}L^{-1}$, inert atmosphere at 40 °C. The concentration Cr(VI) in the wastewaters of most industrial emission sources is estimated to be between 0.1 and 200 $mg{\cdot}L^{-1}$; therefore an initial Cr(VI) concentration of 50 $mg{\cdot}L^{-1}$ was taken as the well-representative mean value of Cr(VI) content in many industrial wastewaters.

Fig. 4 reports removal efficiency results ($mg_{Cr}{\cdot}g^{-1}$) as a function of Sn loading for both Sn/HAP sample series. It is worth stressing that under these specific conditions an analogous reduction process in homogeneous conditions would be associated with electric potential values between 1.4 and 1.45 V, depending on Sn loading. Even if important differences can be guessed in the electrochemical potential of Sn(II) species in Sn/HAP, the reduction of Cr(VI) by Sn(II), even when immobilized on HAP, should be a spontaneous process from a thermodynamic point of view.

Two different trends were observed for the Sn/HAP_{coll} and Sn/HAP_{sol} series samples. In the case of Sn/HAP_{coll}, the removal efficiency linearly increased with Sn loading to reach the total Cr removal (*ca* 10 $mg_{Cr}{\cdot}g^{-1}$) with Sn7.5/HAP sample. Total efficiency was maintained also for higher Sn loading (*i.e*, Sn10/HAP_{coll}). Conversely, in the case of Sn/HAP_{sol} series samples, a *volcano*-like profile was obtained (with maximum of *ca*. 7 $mg_{Cr}{\cdot}g^{-1}$) without attainment of total removal.

Such difference of activity between the two series samples may be explained in terms of different Sn morphology and concentration at the surface.

The above-reported HAADF-STEM images (Figs. 2 and 3) supported the idea that larger aggregates are present in Sn/HAP_{sol} samples compared to Sn/HAP_{coll} ones, mainly containing small and highly dispersed Sn nanoparticles. This difference in the observed Sn morphologies could become ever more pronounced with the increasing Sn loading. The drop of Cr(VI)-removal capacity observed for Sn7.5/HAP_{sol} to Sn10/HAP_{sol} (Fig. 4) could be then due to different intrinsic activity of the two types of Sn phases.

To verify the Sn dispersion at the surface of each sample and the surface chemical composition, the samples were analyzed by X-ray photoelectron spectroscopy (XPS). Chosen samples were also analyzed after use.

Table 1 reports the surface composition of selected Sn/HAP samples comparing samples obtained with the two procedures of Sn-deposition on HAP.

The Ca/P atomic ratio calculated from XPS data was found to be 1.96

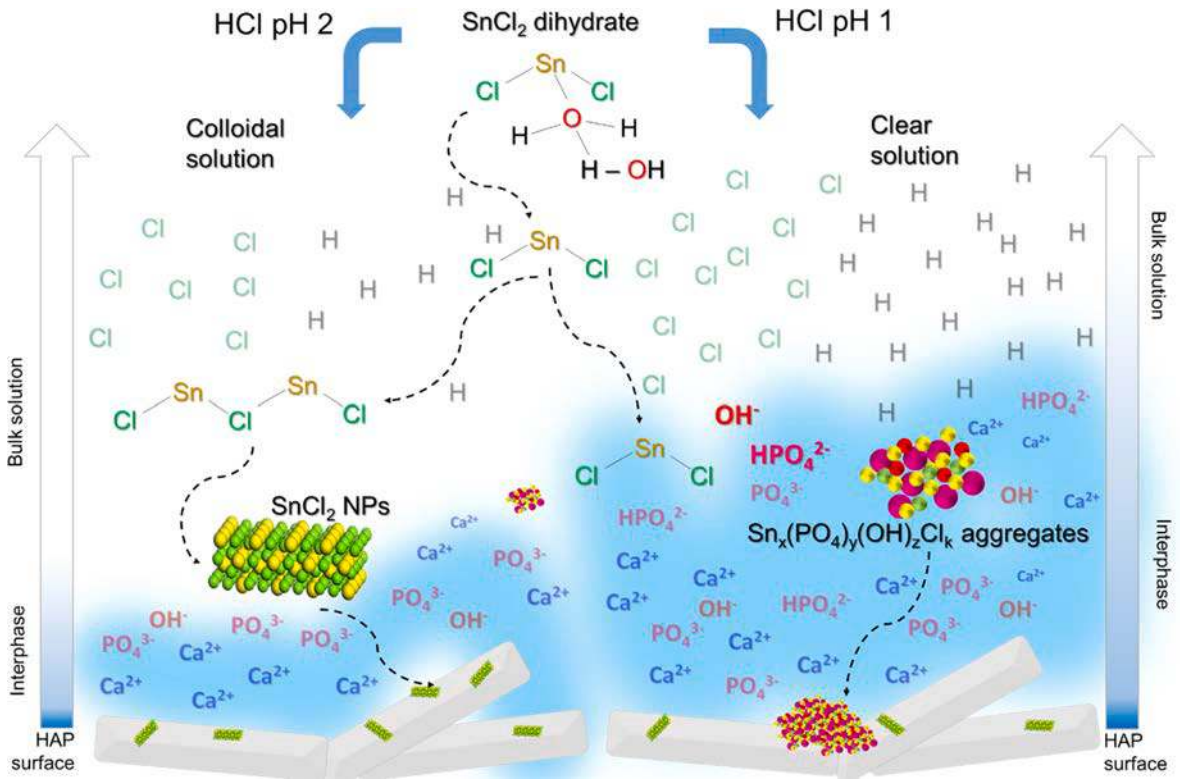

Scheme 1. Formation of Sn-NPs, (from $SnCl_2$ solution at pH = 2) and $Sn_x(PO_4)_y(OH)_zCl_k$ aggregates (from $SnCl_2$ solution at pH = 1) on the HAP surface leading to Sn/HAP_{coll} and Sn/HAP_{sol}, sample series, respectively.

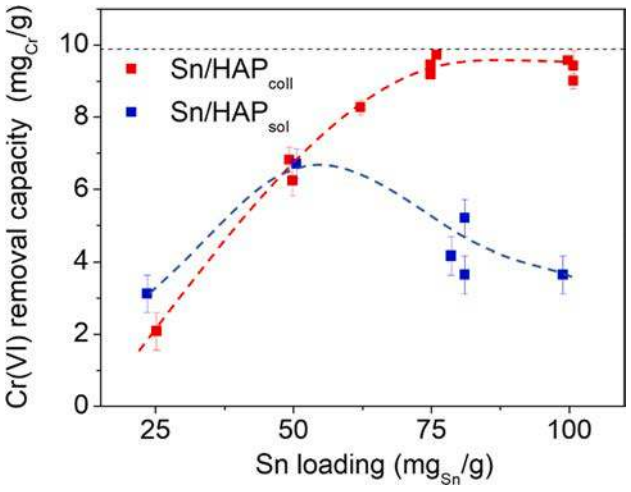

Fig. 4. Cr(VI) removal capacity of Sn/HAP_{coll} and Sn/HAP_{sol} samples as a function of Sn loading ($[Cr(VI)]^{\circ}$=50 mg·L^{-1}, pH = 3, Sn/HAP dosage = 4 g·L^{-1}, inert atmosphere). Dotted line represents total removal corresponding to initial Cr(VI) concentration in solution.

for bare HAP, higher than for stoichiometric HAP, i.e., 1.67. This can be justified considering that bare hydroxyapatite has a higher concentration of calcium at the surface compared to bulk crystal lattice. The Ca/P ratio falls down to 1.46 in the two Sn7.5/HAP samples (Table 1) and to about 1.6 in the Sn5/HAP ones. The Ca/P ratio variation reflected the decrease in the surface concentration of Ca with the added Sn amount. This would suggest the occurrence of surface reconstruction and rearrangements of the first layers of HAP during the Sn-deposition with Ca (II) ion sinking in the deeper layers of the HAP surface.

Interestingly, the surface concentration of Sn was similar for $Sn5/HAP_{coll}$ (6.6%) and $Sn5/HAP_{sol}$ (6.2%), while a marked discrepancy appeared comparing $Sn7.5/HAP_{coll}$ (9.4%) and $Sn7.5/HAP_{sol}$ (7.7%). The values of Sn dispersion can be quantitatively evaluated from the Sn/(Ca + P) ratios, whose values in Table 1 confirm a higher Sn dispersion for Sn/HAP_{coll} samples, in particular at higher Sn-concentration (0.42 for $Sn7.5/HAP_{coll}$). The important information from XPS corroborated the hypothesis that the unexpected trend observed for the Sn/HAP_{sol} series samples, observed in Fig. 4, can be ascribable to the decrease in Sn dispersion with Sn loading, as a consequence of the formation of large aggregates as evidenced by electron microscopy analysis.

Fig. 5A shows the wide-scan spectra of the Sn-richest fresh and used samples in which the presence of O, C, Ca, P, Sn and Cr elements is indicated. The Cr element was observed only for the used samples indicating that the Cr species are undoubtedly adsorbed on the studied solids. The strongest intensity of the Cr 2p peak is observed for $Sn7.5/HAP_{coll}$ compared to $Sn7.5/HAP_{sol}$, indicating its highest adsorption capacity towards Cr species, also in agreement with the higher surface concentration of Sn able to reduce a higher amount of Cr(VI) species (Table 1). This is also evident from the surface (Cr + Sn)/(Ca + P) ratio (Table 1) of the used samples ($Sn7.5/HAP_{coll}$ and $Sn7.5/HAP_{sol}$), which indicates a higher value for the more active sample in the Cr(VI) reduction-immobilization process (Fig. 4), as expected.

In Fig. 5B-F are reported, respectively, the O 1s, Cr 2p, Sn 3d, Ca 2p, and P 2p regions of the XPS spectrum of $Sn7.5/HAP_{coll}$ used sample.

Two fitted peaks were confirmed in the high-resolution 1s core level of O for all samples, as presented in Fig. 5B, wherein the peaks at around 531 and 533 eV were assigned to the crystal lattice oxygen in HAP and hydroxyl group on adsorbent surface, respectively [57].

Fig. 5D reveals the high-resolution X-ray photoelectron spectrum of the Sn 3d. Two peaks are observed (splitting of spin orbit) characteristic to Sn $3d_{5/2}$ and Sn $3d_{3/2}$ located, for the studied samples, at binding energy between 486.7–487.2 eV and 495.1–495.6 eV, respectively, without the possibility to distinguish between +2 and +4 oxidation states.

Table 1
Surface composition of the samples obtained from XPS analysis.

Sample code	Surface composition/atomic %											
	Fresh sample					Sample after use						
	Sn	Ca	P	O	Sn/(Ca + P)	Sn	Cr	Ca	P	O	Sn/(Ca + P)	(Sn + Cr)/(Ca + P)
HAP[1]	–	20.3	10.4	69.3	–	–	–	–	–	–	–	–
$Sn5/HAP_{coll}$	6.6	15.0	9.4	68.9	0.27	–	–	–	–	–	–	–
$Sn5/HAP_{sol}$	6.2	15.1	9.4	69.3	0.25	–	–	–	–	–	–	–
$Sn7.5/HAP_{coll}$	9.4	13.4	9.2	68.0	0.42	6.5	2.4	11.4	8.5	71.2	0.33	0.45
$Sn7.5/HAP_{sol}$	7.7	14.4	10.0	67.9	0.32	2.5	1.3	16.5	10.0	69.7	0.09	0.16

[1] Ca/P at surface = 1.96.

The binding energies of the Ca $2p_{3/2}$ and P 2p peaks at about 347 and 133 eV, respectively, agree with the values generally reported for HAP [58].

Fig. 5E shows the high-resolution Ca 2p XPS spectrum of the used $Sn7.5/HAP_{coll}$. The peaks of Ca $2p_{3/2}$ and Ca $2p_{1/2}$ located, for the bare HAP at 346.9 and 350.5 eV, slightly shift towards higher binding energies (e.g. 347.1 and 350.7 eV in $Sn7.5/HAP_{coll}$) following the addition of tin, while the spin-orbit splitting is maintained of 3.6 eV.

Further, the high-resolution P 2p peak is centered at 133.0 eV for HAP and 133.1–133.2 eV for Sn/HAP fresh and used samples except for the used $Sn7.5/HAP_{coll}$ (Fig. 5F) for which the P 2p peak is detected at 134.8 eV. The shift of binding energy of P 2p component (shift of 1.6 eV compared to bare HAP and Sn/HAP fresh samples), is likely due to decrease of the electronic state density around phosphorus atoms and larger polarization of the P-O bond likely due to Cr(III) presence on HAP surface [59].

For the Cr 2p spectra (Fig. 5C), the $2p_{3/2}$ and $2p_{1/2}$ doublet pair of used $Sn7.5/HAP_{coll}$ can be decomposed into two pairs located at 577.58–587.08 eV (main) and 581.02–590.42 eV, with the relative contributions of 1.89 and 0.26 at%, respectively. The main pair with the peak separation between $2p_{3/2}$ and $2p_{1/2}$ of 9.5 eV can be attributed to the Cr(III) oxidation state [60–62]. Concerning the very weak peaks occurring at higher binding energy (581.02–590.42 eV), they may be assigned to the presence of trace amount of chromium in Cr(VI) oxidation state on the surface of spent $Sn7.5/HAP_{coll}$ [63].

These results suggest that the Cr(VI) reduction process occurs at the interface between Cr(VI) and the surface of Sn/HAP; the Cr(III) formed from the redox process immediately is stabilized on the surface near a Sn-site through the strong coordination interactions with the electron-rich HAP surface functionalities (Scheme 2).

To confirm further the nature and mechanism of the reduction and immobilization process, HAADF-STEM microscopy coupled with EDX analysis was carried out on the $Sn7.5/HAP_{coll}$ sample after the reduction-adsorption test (Fig. 6). Interestingly, the nanoparticles of Sn found onto the surface of the fresh sample are still present after use without significant variations in the average dimensions. This important evidence suggests that the reduction and immobilization process does not alter the size of the Sn-based nanoparticles, which have been beneficially anchored and stabilized on the HAP support and encounter neither an agglomeration phenomenon nor leaching phenomena. This evidence supports the absence of leaching observed by leaching tests carried out on Sn/HAP in aqueous solution at different pH.

From the HAADF-STEM/EDX map, it is clear that the immobilized chromium is well dispersed all over the sample (Fig. 6B). This evidence is in agreement with the already discussed reduction-immobilization mechanism, displayed in Scheme 2.

Finally, reduction-immobilization tests were performed under isothermal mode (T = 40 °C) selecting one sample from Sn/HAP_{coll} series ($Sn10/HAP_{coll}$). Isothermal curve obtained is reported in Fig. S-9. Among the different equation models used to fit the experimental points, Langmuir model was found the best. This suggested the homogeneous presence of Sn-centers on HAP able to reduce Cr(VI), as observed also by STEM microscopy (Fig. 2).

3.2.2. Effect of some operating conditions, kinetics and reusability

Based on the promising performances of Sn/HAP_{coll} samples, deeper investigation of this series was performed, focusing the study on the effect of some relevant operating conditions of reduction-immobilization process of Cr(VI), with the aim to evaluate the potential practical applications of these samples.

First, the effect of atmosphere and in particular the eventual role of dissolved oxygen was investigated. Temperature, Cr(VI) initial concentration, dosage, and pH were kept constant, and instead in inert atmosphere tests of Cr(VI) removal were carried out under the presence of synthetic air fluxing. Surprisingly, the plot of removal capacity as a function of tin concentration on HAP reproduced the same trend as that obtained under inert atmosphere (Fig. 7A). Thus, under the selected conditions, the O_2 dissolved from air at atmospheric pressure into the aqueous acid solution did not influence the Cr(VI) redox process.

Furthermore, the influence of pH was studied by carrying out tests at natural pH. Hydroxyapatite has an amphoteric surface and in water it generates pH = 7. Cr(VI) reducing activity was maintained also under neutral conditions, although a decrease of the performances of the Sn/HAP_{coll} samples was observed (Fig. 7B). The decrease of activity of the samples in non-acidic solutions was foreseeable knowing that the reduction of Cr(VI) with Sn(II) requires an acidic environment (Eq. (1)). Predictably, when a lower initial concentration of Cr(VI) (25 $mg{\cdot}L^{-1}$ instead than 50 $mg{\cdot}L^{-1}$) was used, a smaller amount of Sn was required to completely reduce and remove Cr(VI) from solution. Fig. 7C indicates that little more than 50 $mg_{Sn}{\cdot}g^{-1}$ was sufficient to completely remove chromium from solution.

Concerning kinetics of the reduction-immobilization process, it seemed very rapid by observing the fast discoloration of the pale yellow bichromate solution. Specifically, reaction rate was evaluated for $Sn7.5/HAP_{coll}$ at various temperatures in the 5–40 °C interval. It was found that Cr(VI) reduction rate increased of ca. 20% from 5 °C to 40 °C, passing from 0.01 mmol h^{-1} to 0.012 mmol h^{-1}.

The performance of Cr(VI) reduction of the Sn/HAP samples was also tested after long exposure to the atmosphere. A decline from 85% to 58% was observed after 15 days (Fig. 7D) likely due to the partial oxidation of Sn(II) to Sn(IV).

In addition, reusability tests (Fig. S-10) were explored using $Sn5/HAP_{coll}$ following the operative protocol described in the Experimental section. A drastic drop in the efficiency of Cr(VI) removal after the first run was observed. Comparing the cumulative removal efficiency of $Sn5/HAP_{coll}$ obtained over several runs in independent tests performed at different initial Cr(VI) concentration (25 or 50 $mg{\cdot}L^{-1}$), it appears clear that the sample had worked approaching a given "ceiling value" of Cr (VI) removal (8 $mg_{Cr}{\cdot}g^{-1}$).

Leaching tests on the used materials revealed that both Sn and Cr species are not released in solution (Fig. S-10, b), therefore the low reusability of Sn/HAP is not ascribable to low stability and loss of Sn. Far more likely, the oxidation of Sn(II) to Sn(IV) and the partial blocking of some surface Sn sites by the adsorbed Cr(III) species could be guessed to be responsible for the lack of reusability.

The regeneration of used materials represents, then, a critical issue since a chemical regeneration process should be developed to reduce

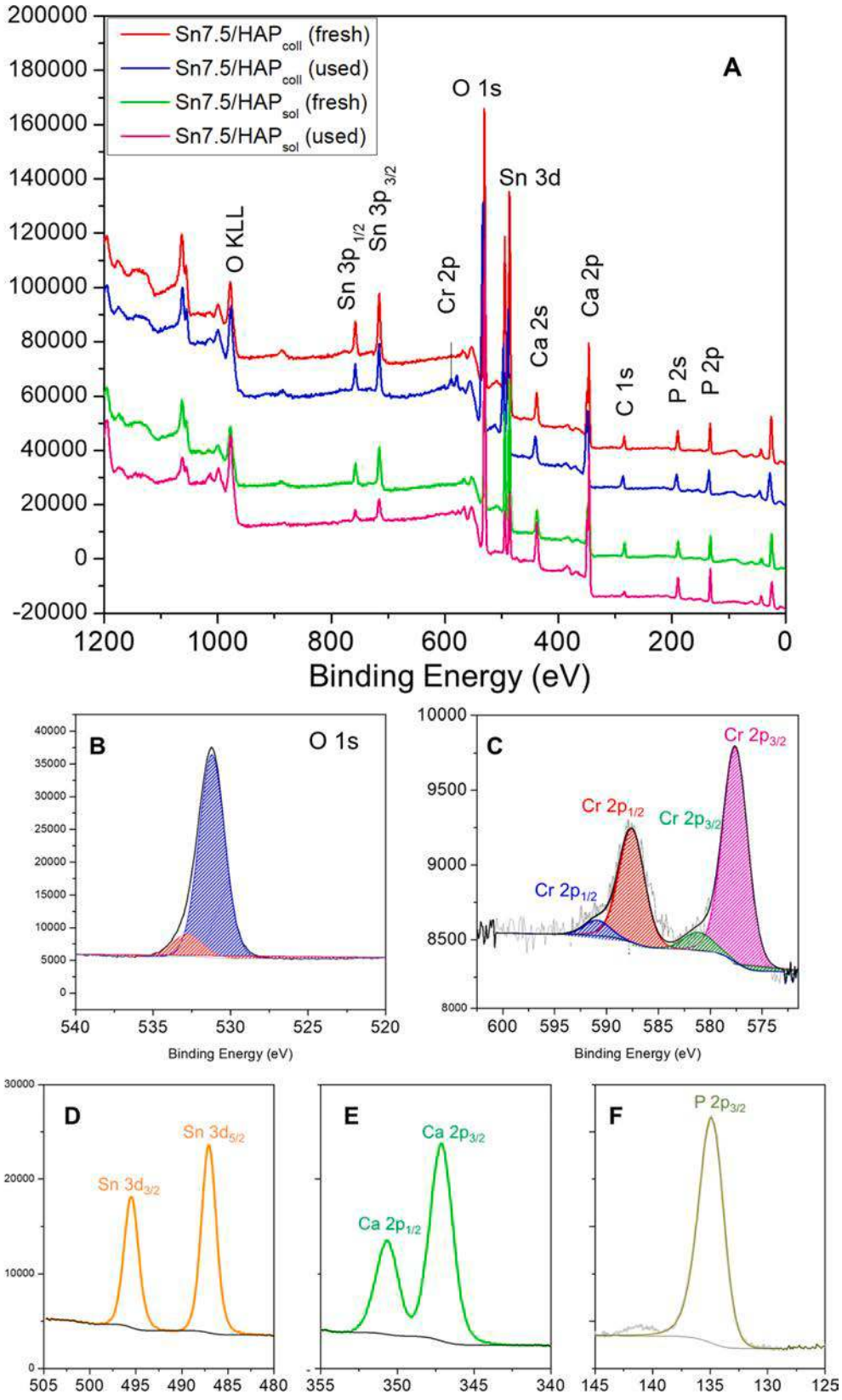

Fig. 5. Full-range XPS spectra of fresh and used Sn7.5/HAP$_{coll}$ and Sn7.5/HAP$_{sol}$ samples, (A); XPS spectra of O 1s, Cr 2p, Sn 3d, Ca 2p and P 2p of used Sn7.5/HAP$_{coll}$ sample, (B-F).

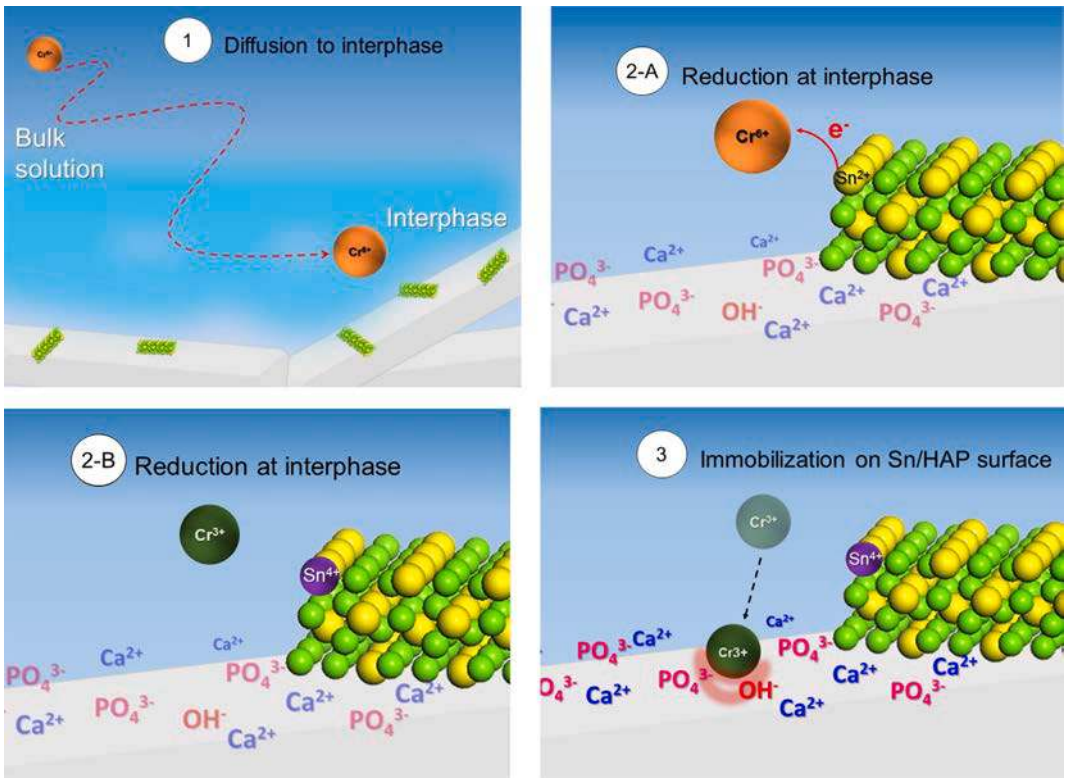

Scheme 2. Interfacial redox process of Cr(VI) with Cr(III) adsorption at Sn/HAP_{coll} surface: diffusion of Cr(VI) from bulk solution to interfacial Sn(II) blocked on HAP, (step 1); electron exchange between Sn(II) and Cr(VI), (step 2-A); formation of Cr(III) in solution and Sn(IV) at HAP surface, (step 2-B); immobilization of Cr(III) at HAP surface, (step 3).

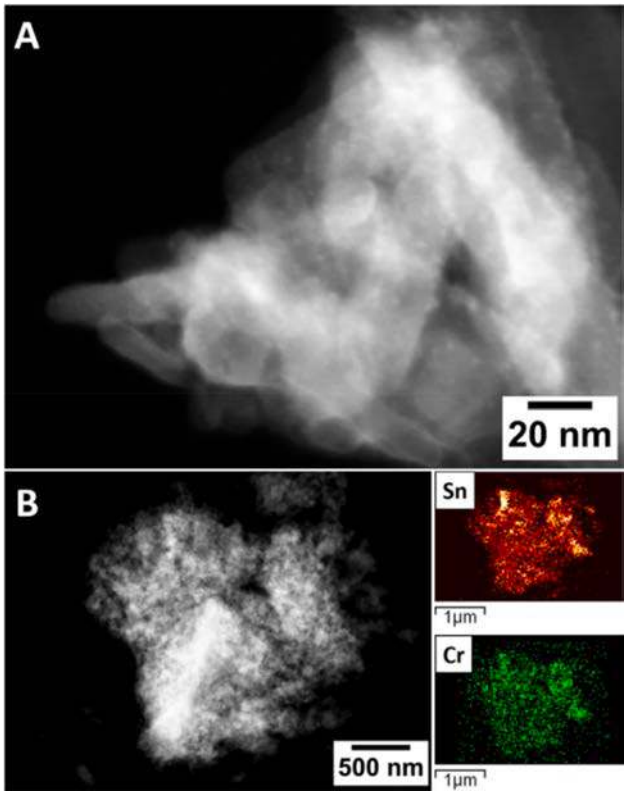

Fig. 6. HAADF-STEM micrograph (A) and HAADF-STEM/EDX mapping of Sn and Cr (B) of used Sn7.5/HAP_{coll}.

formed Sn(IV) to Sn(II) and simultaneously remove adsorbed Cr(III) ions saturating HAP surface. A similar approach would be expensive and difficult to implement. However, to avoid costly disposal of the materials after their use, an alternative to the regeneration could be the valorisation of used materials as catalyst in environmental protection reactions. This strategy is currently under investigation and it will be presented in the next future.

3.2.3. Comparison with other materials

A valid comparison of the performances of our Sn/HAP samples with other competitors proposed in the literature, although not trivial, can help in highlighting the added-value as well as any downsides of our studied materials. The peculiarity of Sn/HAP material lies in the combination of the sorption properties of HAP with the reducing power of Sn (II) species. Most adsorbents, except biochar, exhibit a low adsorption capacity towards Cr(VI) (Table 2, entries 1–7), and a further modification or functionalization of adsorbent surface is necessary to obtain effective materials for Cr(VI) direct adsorption. Hydroxyapatite, as well, possesses a low capability to immobilize Cr(VI). A significant enhancement of adsorption capacity was attained by using cellulose supported magnetic composites, namely iron-oxide coated cellulose/hydroxyapatite (Fe_3O_4@CelHAp) [43]. Conversely, several adsorbents show excellent performances in immobilizing Cr(III) species. On the other hand HAP showed a remarkable capability to adsorb Cr(III) from aqueous solutions, operating the immobilization at the HAP surface with different mechanisms depending on the pH value [32]. The effectiveness of HAP emerges more clearly when the adsorption capacity is normalized respect to the surface area of the solid adsorbent. In this case, HAP shows performances comparable even to the ones of commercial zeolites, Amberlite, boehmite, or kaolin.

However, a more exhaustive comparison must take into account the overall reduction/immobilization process of Cr(VI) to Cr(III). Table 3 compares the Cr(VI) removal capacity of different metal based materials

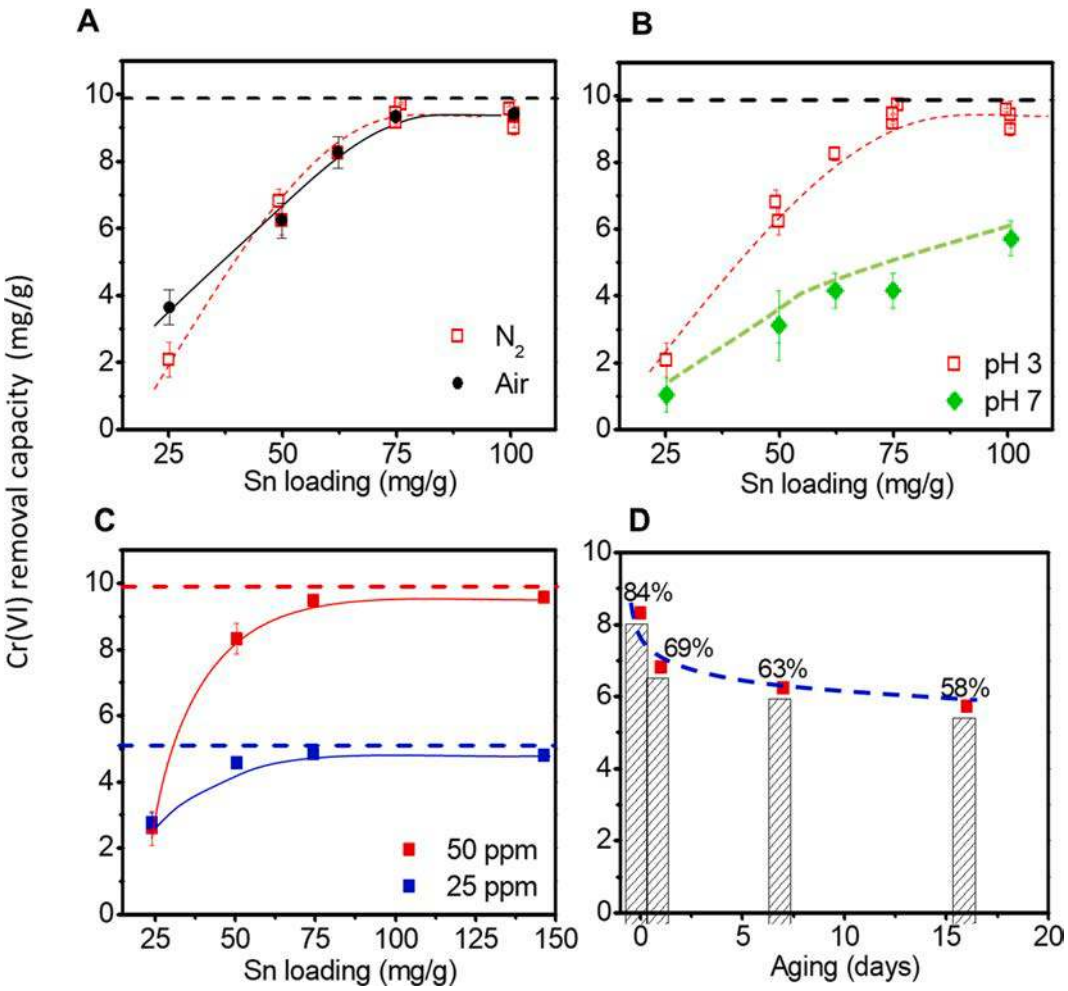

Fig. 7. Influence of some operating conditions on Sn/HAP_{coll} ability in Cr(VI) removal; effect of the atmosphere during reduction (50 mg·L^{-1} of Cr(VI) in 22 mL solution, pH 3, Sn/HAP_{coll} dosage: 4 g·L^{-1}) under inert (N_2) or oxidative (Air) fluxing, (A); effect of pH (50 mg·L^{-1} of Cr(VI in 22 mL solution), (B); effect of initial Cr (VI) concentration (25 or 50 mg·L^{-1} of Cr(VI) solutions at pH 3 and Sn/HAP dosage: 4 g·L^{-1}), (C); aging effect of Sn5/HAP_{coll} in Cr(VI) reduction (50 mg·L^{-1} of Cr(VI) in 22 mL solution, pH 3, Sn/HAP_{coll} dosage: 4 g·L^{-1}), (D). Horizontal dotted lines represent the corresponding maximum removal capacity.

Table 2
Comparison of adsorption capacities for Cr(VI) or Cr(III) of various solid adsorbents.

Type of adsorbent	Surface area/m^2 g^{-1}	Species	Dosage/g_{solid} $L^{-1}{}_{sol}$	Adsorption capacity		Ref.
				/mg_{Cr} g^{-1}_{solid}	/mg_{Cr} $m^{-2}{}_{solid}$	
Activated carbon	853	Cr(VI)	2	13.75	0.016	[64]
Biochar from wheat straw	26	Cr(VI)	4	14.8	0.56	[65]
Nano alumina	79	Cr(VI)	4	8.5	0.11	[66]
Acid activated kaolinite	16	Cr(VI)	2	8.0	0.51	[67]
Hexadecyltrimethylammonium bromide (HDTMA) modified red clay	4	Cr(VI)	4	4.3	0.94	[68]
Hexadecylpyridinium bromide (HDPB) modified chabazite	25	Cr(VI)	5	14.3	2.86	[69]
Tetraoctylammonium bromide impregnated Amberlite XAD-4	825	Cr(VI)	5	196.0	0.24	[70]
Fe_3O_4@CelHAp	102	Cr(VI)	2	25.01	0.24	[43]
Natural mordenite	277	Cr(III)	5	10.92	0.039	[71]
Kaolin	15	Cr(III)	5	7.80	0.52	[71]
Commercial zeolite Z13X	578	Cr(III)	5	183.03	0.32	[71]
Commercial Norit carbon post-oxidized	837	Cr(III)	4	52.52	0.063	[72]
Boehmite Nanoplates	52.22	Cr(III)	1	19.85	0.38	[73]
Hydroxyapatite (suspension at pH = 4)	85	Cr(III)	10	15.6	0.18	[32]
Hydroxyapatite (suspension at pH = 7)	85	Cr(III)	10	26.0	0.31	[32]
Hydroxyapatite (suspension at pH = 9)	85	Cr(III)	10	26.0	0.31	[32]

Table 3
Comparison of Cr(VI) removal capacities of various materials.

Type of material	Synthesis limitations	Removal capacity		Ref.
		$mg_{Cr}\ g_{ads}^{-1}$	$mg_{Cr}\ g_{Me}^{-1}$	
Resin-supported ferragel	Use of synthetic resin as support; use of $NaBH_4$ as reducing agent	6.24	28	[74]
Micron Fe	Control of NP size; use of $NaBH_4$ as reducing agent	1.75	1.75	[75]
Sodium carboxymethyl cellulose-stabilized Fe nanoparticles	Use of $NaBH_4$ as reducing agent	252	252	[76]
Scrap iron	Lack of homogeneity in properties of different iron shaving batches	19.2	19.2	[77]
Zerovalent iron nanoparticles	Use of $NaBH_4$; aggregation.	180	180	[78]
Nano-scale Fe^0 particles supported on a PAA/PVDF membrane	Time-consuming and expensive synthesis of the membrane	n.d.*	181	[79]
Fe^0 nanoparticles synthesized in ethanol–water mixed system	Use of PEG, ethanol and $NaBH_4$	n.d.*	112	[80]
Chitosan-stabilized Fe^0 nanoparticles	Time consuming (24 h) ; use of KBH_4.	n.d.*	148	[80]
Nanoscale zero-valent iron in chitosan beads	Time consuming (24 h); use of acetic acid.	1.3	4	[81]
Silica fume supported-Fe^0 nanoparticles	Use of commercial silica; multistep synthesis; use of ethanol and $NaBH_4$	13	88	[82]
Fe_3O_4-stabilized Fe^0 nanoparticles	Use of KBH_4.	5	348	[83]
$Fe@SiO_2$	Multistep synthesis; delicate control of nucleation; use of ethanol, TEOS and KBH_4	n.d.*	467	[84]
Fe(II)/Stevensite	Multistep synthesis, use of sodium dithionite $Na_2S_2O_4$ as reducing agent	133.7	5.1	[85]
$Sn_6O_4(OH)_4$ nanoparticles	Aggregation	7.2	14.8	[46]
Sn/HAP		10	130	This work

* The value cannot be calculated since some data (e.g. Fe loading) are missing in the original reference.

proposed in the literature for the reduction/adsorption of Cr(VI). For comparative purposes, the removal capacity has been expressed for metal unit ($mg_{Cr} \cdot g_{Me}^{-1}$). Only a few studies reported the use of Sn-containing materials and the most of the competitors in this case are iron-based materials. It emerges that, Sn/HAP (*entry15*, 130 $mg_{Cr} \cdot g_{Me}^{-1}$ removal) is among the most effective materials. In addition, it takes advantage from the unique features of biocompatibility and easy synthetic preparation starting from eco-friendly and bioavailable materials.

4. Conclusions

In summary, we presented Sn-functionalized hydroxyapatite as an innovative and effective eco-friendly material for the removal of toxic Cr (VI) species with a reduction/immobilization process. Cr(VI) removal capacity increased with Sn-concentration deposited on HAP starting from colloidal solutions of tin chloride.

The pH influenced both Sn-speciation in solution and interfacial properties of hydroxyapatite, therefore, materials with different surface concentration and morphology of the Sn phase have been prepared and studied.

Combined transmission electron microscopy and XPS investigation provided valuable evidences of the mechanism of Cr(VI) removal, consisting in the reduction of Cr(VI) by Sn(II) phase anchored on HAP surface, followed by immobilization of the formed Cr(III) species at the Sn/HAP interphase.

Based on the comparison to other competitors, Sn/HAP materials appear as promising candidates for the removal of Cr(VI) from wastewaters taking advantage of their eco-friendliness and facile synthesis, among others positive properties of HAP.

However, further studies are still needed to improve performance and current understanding. Starting from the hydroxyapatite, a solid offering higher surface area should be desirable, which might lead to a higher Cr(III) adsorption, thus improving the final material performances in the reduction-immobilization process. Maximizing Sn dispersion on hydroxyapatite by exploring deposition methods alternative to classical wet methods, as well as the development of proper regeneration procedures of the used materials represent two important challenges to be addressed in next steps.

Funding Sources

HeidelbergCement, Bergamo, Italia, supported the start of this activity in 2017 at Dipartimento di Chimica, Università degli Studi di Milano, Italy, with a research contract.

CRediT authorship contribution statement

Sebastiano Campisi: Conceptualization, Methodology, Writing - original draft. **Claudio Evangelisti:** Investigation. **Georgeta Postole:** Investigation. **Antonella Gervasini:** Supervision, Writing - review & editing.

Declaration of Competing Interest

The authors declare that they have no known competing financial interests or personal relationships that could have appeared to influence the work reported in this paper.

Acknowledgments

A. Gervasini and S. Campisi of the Università degli Studi di Milano would like to thank Dr. Maurizio Marchi, Team Leader at HeidelbergCement Group, Bergamo, Italia, for stimulating discussions on the material design. In addition, the authors acknowledge the valid contribution of Mr. Francesco Panico and Mr. Riccardo Motta. One of the authors (GP) thanks P-P. Bargiela and N. Bonnet for XPS and chemical analyses, respectively. Ljiljana Damjanović-Vasilić, Faculty of Physical Chemistry - University of Belgrade, is acknowledged for fruitful discussions on.

Appendix A. Supplementary data

Supplementary data to this article can be found online at https://doi.org/10.1016/j.apsusc.2020.148227.

References

[1] J. Guertin, J.A. Jacobs, C.P. Avakian, Chromium(VI) Handbook, CRC Press, 2004.
[2] M. Owlad, M.K. Aroua, Removal of hexavalent chromium-contaminated water and wastewater : a review, (2009) 59–77. doi:10.1007/s11270-008-9893-7.
[3] S.S. Tahir, R. Naseem, Removal of Cr(III) from tannery wastewater by adsorption onto bentonite clay, Sep. Purif. Technol. 53 (2007) 312–321, https://doi.org/10.1016/j.seppur.2006.08.008.
[4] C.E. Barrera-Díaz, V. Lugo-Lugo, B. Bilyeu, A review of chemical, electrochemical and biological methods for aqueous Cr(VI) reduction, J. Hazard. Mater. 223–224 (2012) 1–12, https://doi.org/10.1016/j.jhazmat.2012.04.054.
[5] V.E. Pakade, N.T. Tavengwa, L.M. Madikizela, Recent advances in hexavalent chromium removal from aqueous solutions by adsorptive methods, RSC Adv. 9 (2019) 26142–26164, https://doi.org/10.1039/c9ra05188k.
[6] M.L. Peterson, G.E. Brown, G.A. Parks, Direct XAFS evidence for heterogeneous redox reaction at the aqueous chromium/magnetite interface, Colloids Surf. A Physicochem. Eng. Asp. 107 (1996) 77–88, https://doi.org/10.1016/0927-7757(95)03345-9.
[7] G. Bidoglio, P.N. Gibson, M. O'Gorman, K.J. Roberts, X-ray absorption spectroscopy investigation of surface redox transformations of thallium and

chromium on colloidal mineral oxides, Geochim. Cosmochim. Acta 57 (1993) 2389–2394, https://doi.org/10.1016/0016-7037(93)90576-I.
[8] E.S. Ilton, C.O. Moses, D.R. Veblen, Using X-ray photoelectron spectroscopy to discriminate among different sorption sites of Micas: with implications for heterogeneous reduction of chromate at the mica-water interface, Geochim. Cosmochim. Acta 64 (2000) 1437–1450, https://doi.org/10.1016/S0016-7037(99)00372-5.
[9] J. Jian Pan, J. Jiang, R. Kou Xu, Removal of Cr(VI) from aqueous solutions by Na 2 SO 3 /FeSO 4 combined with peanut straw biochar, Chemosphere 101 (2014) 71–76, https://doi.org/10.1016/j.chemosphere.2013.12.026.
[10] X. Lv, Y. Zhang, W. Fu, J. Cao, J. Zhang, H. Ma, G. Jiang, Zero-valent iron nanoparticles embedded into reduced graphene oxide-alginate beads for efficient chromium (VI) removal, J. Colloid Interface Sci. 506 (2017) 633–643, https://doi.org/10.1016/j.jcis.2017.07.024.
[11] R. Yang, Y. Wang, M. Li, Y. Hong, A new carbon/ferrous sulfide/iron composite prepared by an in situ carbonization reduction method from hemp (cannabis sativa L.) stems and its Cr(VI) removal ability, ACS Sustain Chem. Eng. 2 (2014) 1270–1279, https://doi.org/10.1021/sc500092z.
[12] T. Yang, L. Meng, S. Han, J. Hou, S. Wang, X. Wang, Simultaneous reductive and sorptive removal of Cr(VI) by activated carbon supported β-FeOOH, RSC Adv. 7 (2017) 34687–34693, https://doi.org/10.1039/c7ra06440c.
[13] D. Wang, G. Zhang, Z. Dai, L. Zhou, P. Bian, K. Zheng, Z. Wu, D. Cai, Sandwich-like nanosystem for simultaneous removal of Cr(VI) and Cd(II) from water and soil, ACS Appl. Mater. Interfaces 10 (2018) 18316–18326, https://doi.org/10.1021/acsami.8b03379.
[14] X. Lv, X. Qin, K. Wang, Y. Peng, P. Wang, G. Jiang, Nanoscale zero valent iron supported on MgAl-LDH-decorated reduced graphene oxide: enhanced performance in Cr(VI) removal, mechanism and regeneration, J. Hazard. Mater. 373 (2019) 176–186, https://doi.org/10.1016/j.jhazmat.2019.03.091.
[15] X. Lv, G. Jiang, X. Xue, D. Wu, T. Sheng, C. Sun, X. Xu, Fe0-Fe3O4 nanocomposites embedded polyvinyl alcohol/sodium alginate beads for chromium (VI) removal, J. Hazard. Mater. 262 (2013) 748–758, https://doi.org/10.1016/j.jhazmat.2013.09.036.
[16] H. Wang, X. Yuan, Y. Wu, X. Chen, L. Leng, H. Wang, H. Li, G. Zeng, Facile synthesis of polypyrrole decorated reduced graphene oxide-Fe3O4 magnetic composites and its application for the Cr(VI) removal, Chem. Eng. J. 262 (2015) 597–606, https://doi.org/10.1016/j.cej.2014.10.020.
[17] T. Wang, L. Zhang, C. Li, W. Yang, T. Song, C. Tang, Y. Meng, S. Dai, H. Wang, L. Chai, J. Luo, Synthesis of core-shell magnetic Fe3O4@poly(m -phenylenediamine) particles for chromium reduction and adsorption, Environ. Sci. Technol. 49 (2015) 5654–5662, https://doi.org/10.1021/es5061275.
[18] X. Guan, Y. Chen, H. Fan, Stepwise deprotonation of magnetite-supported gallic acid modulates oxidation state and adsorption-assisted translocation of hexavalent chromium, ACS Appl. Mater. Interfaces 9 (2017) 15525–15532, https://doi.org/10.1021/acsami.7b03061.
[19] W. Jiang, Q. Cai, W. Xu, M. Yang, Y. Cai, D.D. Dionysiou, K.E. O'Shea, Cr(VI) adsorption and reduction by humic acid coated on magnetite, Environ. Sci. Technol. 48 (2014) 8078–8085, https://doi.org/10.1021/es405804m.
[20] B. Qiu, J. Guo, X. Zhang, D. Sun, H. Gu, Q. Wang, H. Wang, X. Wang, X. Zhang, B. L. Weeks, Z. Guo, S. Wei, Polyethylenimine facilitated ethyl cellulose for hexavalent chromium removal with a wide pH range, ACS Appl. Mater. Interfaces. 6 (2014) 19816–19824, https://doi.org/10.1021/am505170j.
[21] N. Shevchenko, V. Zaitsev, A. Walcarius, Bifunctionalized mesoporous silicas for Cr (VI) reduction and concomitant Cr(III) immobilization, Environ. Sci. Technol. 42 (2008) 6922–6928, https://doi.org/10.1021/es800677b.
[22] Y. Ying, Y. Liu, X. Wang, Y. Mao, W. Cao, P. Hu, X. Peng, Two-dimensional titanium carbide for efficiently reductive removal of highly toxic chromium(VI) from water, ACS Appl. Mater. Interfaces 7 (2015) 1795–1803, https://doi.org/10.1021/am5074722.
[23] F.Q. Shao, J.J. Feng, X.X. Lin, L.Y. Jiang, A.J. Wang, Simple fabrication of AuPd@Pd core-shell nanocrystals for effective catalytic reduction of hexavalent chromium, Appl. Catal. B Environ. 208 (2017) 128–134, https://doi.org/10.1016/j.apcatb.2017.02.051.
[24] N. Daneshvar, D. Salari, S. Aber, Chromium adsorption and Cr(VI) reduction to trivalent chromium in aqueous solutions by soya cake, J. Hazard. Mater. 94 (2002) 49–61, https://doi.org/10.1016/S0304-3894(02)00054-7.
[25] D. Park, S.R. Lim, Y.S. Yun, J.M. Park, Reliable evidences that the removal mechanism of hexavalent chromium by natural biomaterials is adsorption-coupled reduction, Chemosphere 70 (2007) 298–305, https://doi.org/10.1016/j.chemosphere.2007.06.007.
[26] H.K. Zhang, H. Lu, J. Wang, J.T. Zhou, M. Sui, Cr(VI) reduction and Cr(III) immobilization by acinetobacter sp. HK-1 with the assistance of a novel quinone/graphene oxide composite, Environ. Sci. Technol. 48 (2014) 12876–12885, https://doi.org/10.1021/es5039084.
[27] S. Periyasamy, M. Naushad, N. Viswanathan, Hydrothermal fabrication of triazine-functionalized covalent organic polymer enfolded alginate biocomposite beads for Cr(vi) removal from water, Environ. Sci. Water Res. Technol. 6 (2020) 851–863, https://doi.org/10.1039/c9ew01096c.
[28] M. Zhang, Z. Xu, J. Liang, L. Zhou, C. Zhang, Potential application of novel TiO2/β-FeOOH composites for photocatalytic reduction of Cr(VI) with an analysis of statistical approach, Int. J. Environ. Sci. Technol. 12 (2015) 1669–1676, https://doi.org/10.1007/s13762-014-0533-z.
[29] Z. Xu, S. Bai, J. Liang, L. Zhou, Y. Lan, Photocatalytic reduction of Cr(VI) by citric and oxalic acids over biogenetic jarosite, Mater. Sci. Eng. C 33 (2013) 2192–2196, https://doi.org/10.1016/j.msec.2013.01.040.
[30] R. Djellabi, F.M. Ghorab, S. Nouacer, A. Smara, O. Khireddine, Cr(VI) photocatalytic reduction under sunlight followed by Cr(III) extraction from TiO2 surface, Mater. Lett. 176 (2016) 106–109, https://doi.org/10.1016/j.matlet.2016.04.090.
[31] J.H. Wu, F.Q. Shao, S.Y. Han, S. Bai, J.J. Feng, Z. Li, A.J. Wang, Shape-controlled synthesis of well-dispersed platinum nanocubes supported on graphitic carbon nitride as advanced visible-light-driven catalyst for efficient photoreduction of hexavalent chromium, J. Colloid Interface Sci. 535 (2019) 41–49, https://doi.org/10.1016/j.jcis.2018.09.080.
[32] J.H. Wu, F.Q. Shao, X.Q. Luo, H.J. Xu, A.J. Wang, Pd nanocones supported on g-C 3 N 4: an efficient photocatalyst for boosting catalytic reduction of hexavalent chromium under visible-light irradiation, Appl. Surf. Sci. 471 (2019) 935–942, https://doi.org/10.1016/j.apsusc.2018.12.075.
[33] X. Li, K. Yang, C. Yu, S. Yang, K. Zhang, W. Dai, H. Ji, L. Zhu, W. Huang, S. Ouyang, Advances towards the utilization of Vis-NIR light energy by coating YF3:Yb3+, Er3 + over ZnS microspheres triggering hydrogen production and pollutants disposal, J. Mater. Chem. C 7 (2019) 8053–8062, https://doi.org/10.1039/c9tc02068c.
[34] Y. Tian, L. Huang, X. Zhou, C. Wu, Electroreduction of hexavalent chromium using a polypyrrole-modified electrode under potentiostatic and potentiodynamic conditions, J. Hazard. Mater. 225–226 (2012) 15–20, https://doi.org/10.1016/j.jhazmat.2012.04.057.
[35] X. Mo, Z. Hui Yang, H. Yin Xu, G. Ming Zeng, J. Huang, X. Yang, P. Pei Song, L. Ke Wang, Combination of cathodic reduction with adsorption for accelerated removal of Cr(VI) through reticulated vitreous carbon electrodes modified with sulfuric acid-glycine co-doped polyaniline, J. Hazard. Mater. (2015) 493–502, https://doi.org/10.1016/j.jhazmat.2015.01.002.
[36] H. Wang, C. Na, Binder-free carbon nanotube electrode for electrochemical removal of chromium, ACS Appl. Mater. Interfaces. 6 (2014) 20309–20316, https://doi.org/10.1021/am505838r.
[37] M. Ibrahim, M. Labaki, J.-M. Giraudon, J.-F. Lamonier, Hydroxyapatite, a multifunctional material for air, water and soil pollution control: a review, J. Hazard. Mater. 383 (2020) 121139, https://doi.org/10.1016/j.jhazmat.2019.121139.
[38] S. Campisi, C. Castellano, A. Gervasini, Tailoring the structural and morphological properties of hydroxyapatite materials to enhance the capture efficiency towards copper(II) and lead(II) ions, New J. Chem. 42 (2018) 4520–4530, https://doi.org/10.1039/C8NJ00468D.
[39] M. Ferri, S. Campisi, M. Scavini, C. Evangelisti, P. Carniti, A. Gervasini, In-depth study of the mechanism of heavy metal trapping on the surface of hydroxyapatite, Appl. Surf. Sci. 475 (2019) 397–409.
[40] M. Ferri, S. Campisi, A. Gervasini, Nickel and cobalt adsorption on hydroxyapatite: a study for the de-metalation of electronic industrial wastewaters, Adsorption 25 (2019) 649–660, https://doi.org/10.1007/s10450-019-00066-w.
[41] G. Asgari, A.R. Rahmani, J. Faradmal, A.M. Seid Mohammadi, Kinetic and isotherm of hexavalent chromium adsorption onto nano hydroxyapatite, J. Res. Health Sci. 12 (2012) 45–53.
[42] S. Hokkanen, A. Bhatnagar, E. Repo, S. Lou, M. Sillanpää, Calcium hydroxyapatite microfibrillated cellulose composite as a potential adsorbent for the removal of Cr (VI) from aqueous solution, Chem. Eng. J. 283 (2016) 445–452, https://doi.org/10.1016/j.cej.2015.07.035.
[43] S. Periyasamy, V. Gopalakannan, N. Viswanathan, Fabrication of magnetic particles imprinted cellulose based biocomposites for chromium(VI) removal, Carbohydr. Polym. 174 (2017) 352–359, https://doi.org/10.1016/j.carbpol.2017.06.029.
[44] T. Henrie, S. Plummer, J. Orta, S. Bigley, C. Gorman, C. Seidel, K. Shimabuku, H. Liu, Full-scale demonstration testing of hexavalent chromium reduction via stannous chloride application, AWWA Water Sci. 1 (2019) e1136, https://doi.org/10.1002/aws2.1136.
[45] G. Papadopoulos, T. Asimakidou, D. Karfaridis, I. Kellartzis, G. Vourlias, M. Mitrakas, K. Simeonidis, An optimized Cr(VI)-Removal system using Sn-based reducing adsorbents, Water (Switzerland). 11 (2019), https://doi.org/10.3390/w11122477.
[46] F. Pinakidou, E. Kaprara, M. Katsikini, E.C. Paloura, K. Simeonidis, M. Mitrakas, Sn (II) oxy-hydroxides as potential adsorbents for Cr(VI)-uptake from drinking water: an X-ray absorption study, Sci. Total Environ. 551–552 (2016) 246–253, https://doi.org/10.1016/j.scitotenv.2016.01.208.
[47] D. Zeng, C. Yu, Q. Fan, J. Zeng, L. Wei, Z. Li, K. Yang, H. Ji, Theoretical and experimental research of novel fluorine doped hierarchical Sn_3O_4 microspheres with excellent photocatalytic performance for removal of Cr(VI) and organic pollutants, Chem. Eng. J. 391 (2020) 123607, https://doi.org/10.1016/j.cej.2019.123607.
[48] C. Yu, D. Zeng, Q. Fan, K. Yang, J. Zeng, L. Wei, J. Yi, H. Ji, The distinct role of boron doping in Sn3O4 microspheres for synergistic removal of phenols and Cr(vi) in simulated wastewater, Environ. Sci. Nano 7 (2020) 286–303, https://doi.org/10.1039/c9en00899c.
[49] S. Campisi, M.G. Galloni, F. Bossola, A. Gervasini, Comparative performance of copper and iron functionalized hydroxyapatite catalysts in NH3-SCR, Catal. Commun. 123 (2019) 79–85, https://doi.org/10.1016/j.catcom.2019.02.008.
[50] S. Campisi, M.G. Galloni, S.G. Marchetti, A. Auroux, G. Postole, A. Gervasini, Functionalized iron hydroxyapatite as eco-friendly catalyst for NH3-SCR reaction: activity and role of iron speciation on the surface, ChemCatChem. n/a (2019), https://doi.org/10.1002/cctc.201901813.
[51] E.H. SCHEIN, United States Environmental Protection Agency, Method 7196, 1992, 1992.

[52] D.M. Sherman, K.V. Ragnarsdottir, E.H. Oelkers, C.R. Collins, Speciation of tin ž Sn 2 q and Sn 4 q / in aqueous Cl solutions from 25 8 C to 350 8 C: an in situ EXAFS study, Chem. Geol. 169–176 (2000).
[53] K.J. Jackson, H.C. Helgeson, Chemical and thermodynamic constraints on the hydrothermal transport and deposition of tin: I. Calculation of the solubility of cassiterite at high pressures and temperatures, Geochim. Cosmochim. Acta 49 (1985) 1–22, https://doi.org/10.1016/0016-7037(85)90187-5.
[54] K. Persson, Materials Data on SnCl2 (SG:62) by Materials Project, (2014). doi: 10.17188/1274957.
[55] J. Pirnat, J. Lužnik, Z. Jagličić, Z. Trontelj, Dehydration of Solid SnCl2(OH2)· H2O to SnCl2, Zeitschrift Für Naturforsch. A. 49 (1994) 367, https://doi.org/10.1515/zna-1994-1-254.
[56] K.G. Nelson, C.A. Bainbridge, SnHPO 4 from the reaction of stannous fluoride and hydroxyapatite at a low pH, J. Dent. Res. 52 (1973) 318–321, https://doi.org/10.1177/00220345730520022101.
[57] M.E. Zilm, L. Chen, V. Sharma, A. McDannald, M. Jain, R. Ramprasad, M. Wei, Hydroxyapatite substituted by transition metals: experiment and theory, Phys. Chem. Chem. Phys. 18 (2016) 16457–16465, https://doi.org/10.1039/c6cp00474a.
[58] A.R. Boyd, C. O'Kane, B.J. Meenan, Control of calcium phosphate thin film stoichiometry using multi-target sputter deposition, Surf. Coatings Technol. 233 (2013) 131–139, https://doi.org/10.1016/j.surfcoat.2013.04.017.
[59] G. Alberti, U. Costantino, G. Marletta, O. Puglisi, S. Pignataro, ESCA investigations of amorphous and crystalline zirconium acid phosphates, J. Inorg. Nucl. Chem. 43 (1981) 3329–3334, https://doi.org/10.1016/0022-1902(81)80111-X.
[60] V. Maurice, S. Cadot, P. Marcus, Hydroxylation of ultra-thin films of α-Cr2O3 (0001) formed on Cr(110), Surf. Sci. 471 (2001) 43–58, https://doi.org/10.1016/S0039-6028(00)00880-3.
[61] A. Maetaki, M. Yamamoto, H. Matsumoto, K. Kishi, The preparation of ultra-thin chromium–vanadium oxides on Cu(100) studied by XPS and LEED, Surf. Sci. 445 (2000) 80–88, https://doi.org/10.1016/S0039-6028(99)01044-4.
[62] A. Lippitz, T. Hübert, XPS investigations of chromium nitride thin films, Surf. Coatings Technol. 200 (2005) 250–253, https://doi.org/10.1016/j.surfcoat.2005.02.091.
[63] D.W. Fischer, Soft x-ray band spectra and molecular orbital structure of Cr2O3, CrO3, CrO4−2 and Cr2O7−2, J. Phys. Chem. Solids. 32 (1971) 2455–2480, https://doi.org/10.1016/S0022-3697(71)80093-8.
[64] S.X. Liu, X. Chen, X.Y. Chen, Z.F. Liu, H.L. Wang, Activated carbon with excellent chromium(VI) adsorption performance prepared by acid-base surface modification, J. Hazard. Mater. 141 (2007) 315–319, https://doi.org/10.1016/j.jhazmat.2006.07.006.
[65] A. Tytłak, P. Oleszczuk, R. Dobrowolski, Sorption and desorption of Cr(VI) ions from water by biochars in different environmental conditions, Environ. Sci. Pollut. Res. 22 (2015) 5985–5994, https://doi.org/10.1007/s11356-014-3752-4.
[66] Y.C. Sharma, V. Srivastava, A.K. Mukherjee, Synthesis and application of nano-Al2O3 powder for the reclamation of hexavalent chromium from aqueous solutions, J. Chem. Eng. Data. 55 (2010) 2390–2398, https://doi.org/10.1021/je900822j.
[67] K.G. Bhattacharyya, S. Sen Gupta, Adsorption of chromium(VI) from water by clays, Ind. Eng. Chem. Res. 45 (2006) 7232–7240, https://doi.org/10.1021/ie060586j.
[68] A. Gładysz-Płaska, M. Majdan, S. Pikus, D. Sternik, Simultaneous adsorption of chromium(VI) and phenol on natural red clay modified by HDTMA, Chem. Eng. J. 179 (2012) 140–150, https://doi.org/10.1016/j.cej.2011.10.071.
[69] Y. Zeng, H. Woo, G. Lee, J. Park, Adsorption of Cr(VI) on hexadecylpyridinium bromide (HDPB) modified natural zeolites, Microporous Mesoporous Mater. 130 (2010) 83–91, https://doi.org/10.1016/j.micromeso.2009.10.016.
[70] S. Kalidhasan, A. Santhana Krishna Kumar, V. Rajesh, N. Rajesh, Enhanced adsorption of hexavalent chromium arising out of an admirable interaction between a synthetic polymer and an ionic liquid, Chem. Eng. J. (2013) 454–463, https://doi.org/10.1016/j.cej.2013.02.083.
[71] C. Covarrubias, R. García, R. Arriagada, J. Yánez, M.T. Garland, Cr(III) exchange on zeolites obtained from kaolin and natural mordenite, Microporous Mesoporous Mater. 88 (2006) 220–231, https://doi.org/10.1016/j.micromeso.2005.09.007.
[72] S.I. Lyubchik, A.I. Lyubchik, O.L. Galushko, L.P. Tikhonova, J. Vital, I.M. Fonseca, S.B. Lyubchik, Kinetics and thermodynamics of the Cr(III) adsorption on the activated carbon from co-mingled wastes, Colloids Surf. A Physicochem. Eng. Asp. 242 (2004) 151–158, https://doi.org/10.1016/j.colsurfa.2004.04.066.
[73] W. Cui, X. Zhang, C.I. Pearce, Y. Chen, S. Zhang, W. Liu, M.H. Engelhard, L. Kovarik, M. Zong, H. Zhang, E.D. Walter, Z. Zhu, S.M. Heald, M.P. Prange, J. J. De Yoreo, S. Zheng, Y. Zhang, S.B. Clark, P. Li, Z. Wang, K.M. Rosso, Cr(III) adsorption by cluster formation on boehmite nanoplates in highly alkaline solution, Environ. Sci. Technol. 53 (2019) 11043–11055, https://doi.org/10.1021/acs.est.9b02693.
[74] S.M. Ponder, J.G. Darab, T.E. Mallouk, Remediation of Cr(VI) and Pb(II) aqueous solutions using supported, nanoscale zero-valent iron, Environ. Sci. Technol. 34 (2000) 2564–2569, https://doi.org/10.1021/es9911420.
[75] J. Cao, W.-X. Zhang, Stabilization of chromium ore processing residue (COPR) with nanoscale iron particles, J. Hazard. Mater. 132 (2006) 213–219, https://doi.org/10.1016/j.jhazmat.2005.09.008.
[76] Y. Xu, D. Zhao, Reductive immobilization of chromate in water and soil using stabilized iron nanoparticles, Water Res. 41 (2007) 2101–2108, https://doi.org/10.1016/j.watres.2007.02.037.
[77] M. Gheju, A. Iovi, I. Balcu, Hexavalent chromium reduction with scrap iron in continuous-flow system: Part 1: effect of feed solution pH, J. Hazard. Mater. 153 (2008) 655–662, https://doi.org/10.1016/j.jhazmat.2007.09.009.
[78] X. Li, J. Cao, W. Zhang, Stoichiometry of Cr(VI) immobilization using nanoscale zerovalent iron (nZVI): a study with high-resolution X-Ray photoelectron spectroscopy (HR-XPS), Ind. Eng. Chem. Res. 47 (2008) 2131–2139, https://doi.org/10.1021/ie061655x.
[79] S. Li, T. Li, Z. Xiu, Z. Jin, Reduction and immobilization of chromium(vi) by nano-scale Fe0 particles supported on reproducible PAA/PVDF membrane, J. Environ. Monit. 12 (2010) 1153–1158, https://doi.org/10.1039/B919909H.
[80] B. Geng, Z. Jin, T. Li, X. Qi, Preparation of chitosan-stabilized Fe0 nanoparticles for removal of hexavalent chromium in water, Sci. Total Environ. 407 (2009) 4994–5000, https://doi.org/10.1016/j.scitotenv.2009.05.051.
[81] T. Liu, L. Zhao, D. Sun, X. Tan, Entrapment of nanoscale zero-valent iron in chitosan beads for hexavalent chromium removal from wastewater, J. Hazard. Mater. 184 (2010) 724–730, https://doi.org/10.1016/j.jhazmat.2010.08.099.
[82] Y. Li, Z. Jin, T. Li, S. Li, Removal of hexavalent chromium in soil and groundwater by supported nano zero-valent iron on silica fume, Water Sci. Technol. 63 (2011) 2781–2787, https://doi.org/10.2166/wst.2011.454.
[83] Y. Wu, J. Zhang, Y. Tong, X. Xu, Chromium (VI) reduction in aqueous solutions by Fe3O4-stabilized Fe0 nanoparticles, J. Hazard. Mater. 172 (2009) 1640–1645, https://doi.org/10.1016/j.jhazmat.2009.08.045.
[84] Y. Li, Z. Jin, T. Li, Z. Xiu, One-step synthesis and characterization of core-shell Fe@SiO 2 nanocomposite for Cr (VI) reduction, Sci. Total Environ. 421–422 (2012) 260–266, https://doi.org/10.1016/j.scitotenv.2012.01.010.
[85] A. Benhammou, A. Yaacoubi, L. Nibou, B. Tanouti, Study of the removal of mercury(II) and chromium(VI) from aqueous solutions by Moroccan stevensite, J. Hazard. Mater. 117 (2005) 243–249, https://doi.org/10.1016/j.jhazmat.2004.09.023.